*Cardiovascular Engineering and Technology* (© 2016)
DOI: 10.1007/s13239-016-0264-z

# Time-Resolved Micro PIV in the Pivoting Area of the Triflo Mechanical Heart Valve

BERNHARD M. VENNEMANN,[1,2] THOMAS RÖSGEN,[1] THIERRY P. CARREL,[3] and DOMINIK OBRIST[2]

[1]Institute of Fluid Dynamics, ETH Zürich, Sonneggstrasse 3, 8092 Zurich, Switzerland; [2]ARTORG Center, University of Bern, Bern, Switzerland; and [3]Department of Cardiovascular Surgery, Bern University Hospital, Bern, Switzerland

*(Received 28 October 2015; accepted 26 April 2016)*

Associate Editor Ajit P. Yoganathan oversaw the review of this article.

**Abstract**—The Lapeyre-Triflo FURTIVA valve aims at combining the favorable hemodynamics of bioprosthetic heart valves with the durability of mechanical heart valves (MHVs). The pivoting region of MHVs is hemodynamically of special interest as it may be a region of high shear stresses, combined with areas of flow stagnation. Here, platelets can be activated and may form a thrombus which in the most severe case can compromise leaflet mobility. In this study we set up an experiment to replicate the pulsatile flow in the aortic root and to study the flow in the pivoting region under physiological hemodynamic conditions (CO = 4.5 L/min / CO = 3.0 L/min, f = 60 BPM). It was found that the flow velocity in the pivoting region could reach values close to that of the bulk flow during systole. At the onset of diastole the three valve leaflets closed in a very synchronous manner within an average closing time of 55 ms which is much slower than what has been measured for traditional bileaflet MHVs. Hot spots for elevated viscous shear stresses were found at the flanges of the housing and the tips of the leaflet ears. Systolic VSS was maximal during mid-systole and reached levels of up to 40 Pa.

**Keywords**—$\mu$PIV, Particle image velocimetry, Mechanical heart valve, Triflo furtiva valve, High-speed imaging, Gap flow, Shear stress, Hemodynamics.

## INTRODUCTION

Mechanical heart valve replacements offer a long lifetime. However, they often show unphysiological hemodynamic behavior that severely increases the risk of shear induced blood damage, such as hemolysis and platelet activation. To reduce the thrombogenic behavior of mechanical heart valves, the patients must rely on life-long anticoagulation therapy. Tissue valves yield a more natural blood flow, but are limited in their life time to 10–15 years or even less in young patients.[6] The Lapeyre-Triflo FURTIVA mechanical heart valve,[2,3,5,8,10–13,16,20] which was investigated in this project, aims at combining the favorable hemodynamics of tissue valves with the durability of mechanical heart valves. Its tri-leaflet design promises a life-long heart valve replacement without the need for anticoagulation medication. Regions of high shear stresses which can activate thrombocytes, combined with regions of low flow velocities where activated platelets might aggregate and form a thrombus (which can compromise leaflet mobility) are of special interest for the assessment of a heart valve's thrombogenic behavior.[15] Previous research indicates that classical mechanical heart valve designs show such thrombogenic hot spots[7] in the pivoting area of theses valves. It is the aim of this study to quantitatively assess the hemodynamics in the pivoting area of the Triflo valve (Fig. 1) with respect to shear stress and regions of low velocity.

## MATERIALS AND METHODS

Micro particle image velocimetry ($\mu$PIV) is a quantitative tool to investigate the flow at small scales *in vitro*. Fluorescently labeled and neutrally buoyant particles are seeded in the flow. The particles are advected with the local velocity field and are illuminated with a series of short light pulses. Their position is captured with a camera and the velocity field is then determined from the shift between the particle patterns in two subsequent pictures.

### *Measurement Location*

The Lapeyre-Triflo FURTIVA valve features a novel hinge design that is different from that of clas-

Address correspondence to Bernhard M. Vennemann, Institute of Fluid Dynamics, ETH Zürich, Sonneggstrasse 3, 8092 Zurich, Switzerland. Electronic mail: vennemann@ifd.mavt.ethz.ch



Published online: 13 May 2016

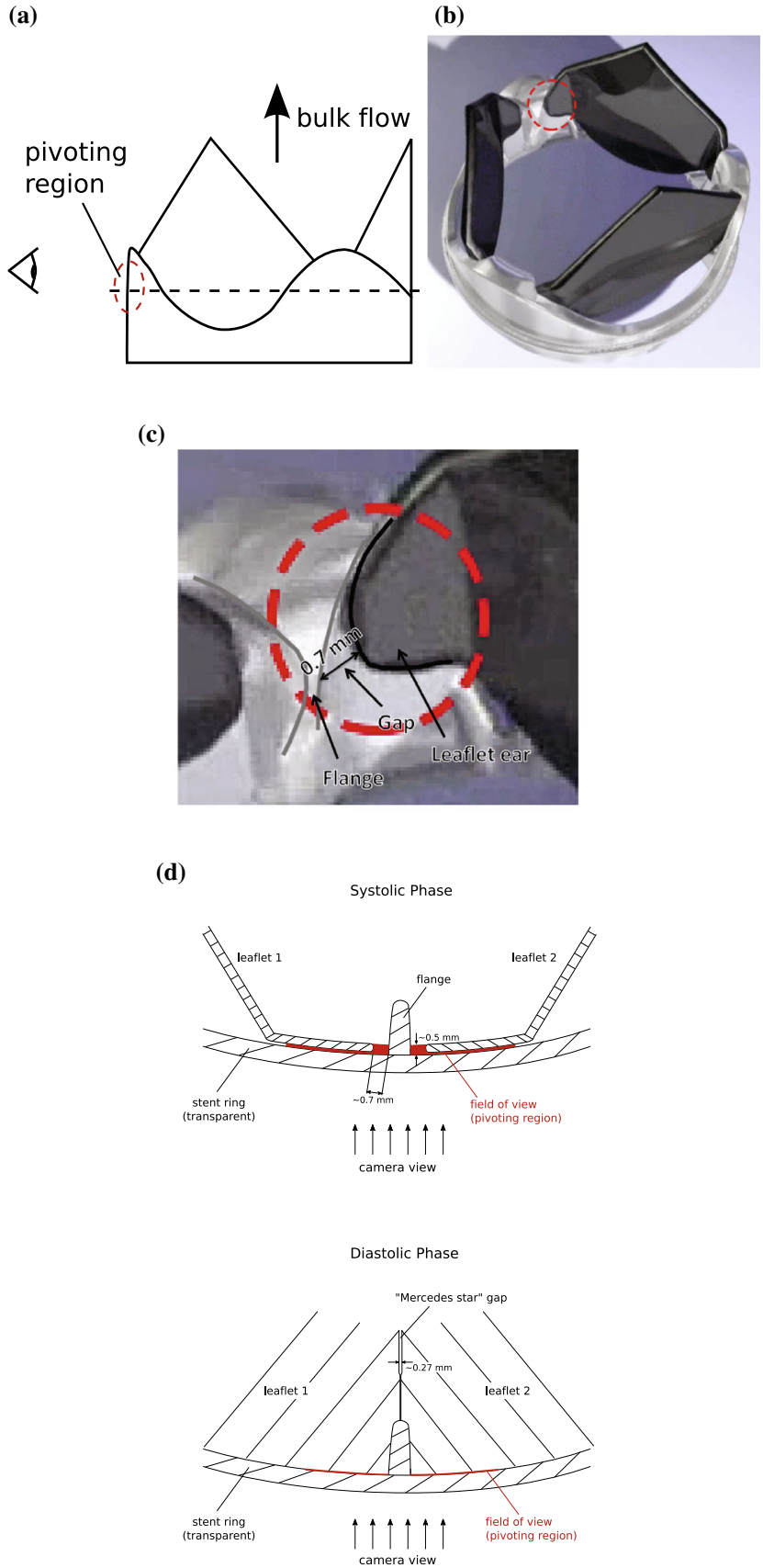
(a)
bulk flow
pivoting region
(b)
(c)
0.7 mm
Gap
Leaflet ear
Flange
(d)
Systolic Phase
leaflet 1
leaflet 2
flange
~0.5 mm
~0.7 mm
stent ring (transparent)
field of view (pivoting region)
camera view
Diastolic Phase
"Mercedes star" gap
~0.27 mm
leaflet 1
leaflet 2
stent ring (transparent)
field of view (pivoting region)
camera view

◀**FIGURE 1. Viewing angle for PIV experiments (a); pivoting region of the valve (b); a close-up of the pivoting region (c) and a sketch [sectional drawing through the pivoting region as indicated by the dashed line in (a)] of the systolic and diastolic geometry with the field of view indicated in red (d).**

sical MHVs. Instead of a hinge mechanism consisting of a recess and a rotating anchor point within, the leaflets have a virtual axis of rotation that lies outside the housing. The leaflets are equipped with small winglets (''leaflet ears'') which hold the leaflets in place while allowing for rotational movement (Fig. 1). The aim of this design is to avoid thrombogenic hot spots in the pivoting region.[4,7,9] (A 3D video animation illustrating the pivoting mechanism of the valve is provided in the supplementary material.) Nevertheless, there exists a narrow clearance during systole between the winglets and the stent ring that may be a region of elevated shear stresses. During diastole this clearance closes because the edges of the winglets fit tightly with the stent ring effectively sealing the pivoting region. This clearance is the region of interest for this study. In the following, we will refer to it as the ''pivoting region'' (Fig. 1d). Figure 2 shows an inverted greyscale image of the measurement plane as seen by the camera.

### *Measurement Setup*

Figure 3 illustrates the experimental setup that was built to investigate the flow under physiological conditions. It is driven by a peristaltic pump (Superpump, Vivitro Systems, Victoria, BC, Canada) (1) which generates a directed pulsatile flow through the test section (3). The net flow through the transparent test section is recorded with a clamp-on flow meter (16PXL, Transonic Systems Inc., Ithaca, NY, USA) (2). The test section holds the Lapeyre-Triflo FURTIVA valve which is mounted in a supra-annular position as recommended for small annulus sizes.[22] Left ventricular pressure (LVP) and aortic pressure (AP) are measured relative to the atmospheric pressure three valve diameters upstream and downstream respectively. The test section is followed by an air chamber compliance (4) to mimic the Windkessel effect. A heat exchanger (5) is incorporated into the flow loop to ensure constant fluid temperature because it has a strong effect on the viscosity and to a lesser degree on the optical refractive index of the blood analog. A fluid reservoir (6) ensures sufficient back-flow through the (mechanical) mitral valve (7). Variable flow resistances (8) are used to fine-tune the pressure profiles to physiological levels. The scene is locally illuminated with a pulsed green high-power LED (9) and is captured by a high-speed camera (10).

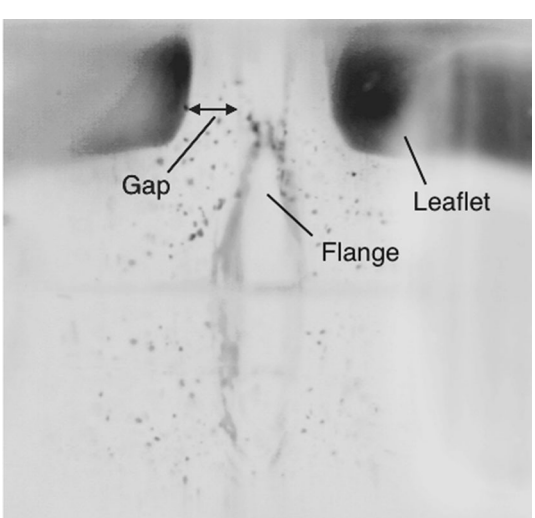


**FIGURE 2. Inverted greyscale image of the measurement location as seen by the camera. A gap exists between leaflet and a flange of the housing during systole.**

### *Valve and Aortic Root Design*

The test section includes the 21mm Lapeyre-Triflo FURTIVA heart valve (Triflo Medical, Neuchâtel, Switzerland) and a model of the aortic root according to Swanson *et al.*[21] In order to gain optical access to the pivoting area (Fig. 1), both valve housing as well as the surrounding vessel structure (i.e. the aortic root) were manufactured from an optically transparent material. Here, a novel 3D-printing approach was pursued in which we equipped a suitable printer (Objet Eden350V, Stratasys Ltd., Eden Prairie, MN, USA) with a transparent printing material (VeroClear, Stratasys Ltd., Eden Prairie, MN, USA). The material is rigid with a Young's modulus of 2000–3000 N/mm$^2$ which is comparable to that of PMMA (2700–3200 N/

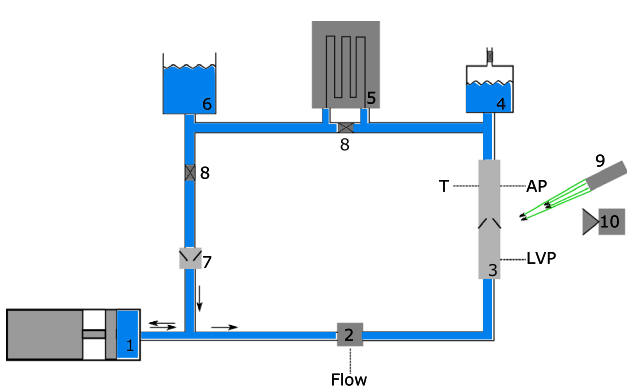


**FIGURE 3. Experimental setup to replicate the flow in the aortic root. (1) Vivitro pulsatile pump, (2) flow meter, (3) test section with Triflo valve, (4) air chamber compliance, (5) heat exchanger, (6) fluid reservoir, (7) mitral valve, (8) variable flow resistance, (9) high-power LED, (10) high-speed camera.**

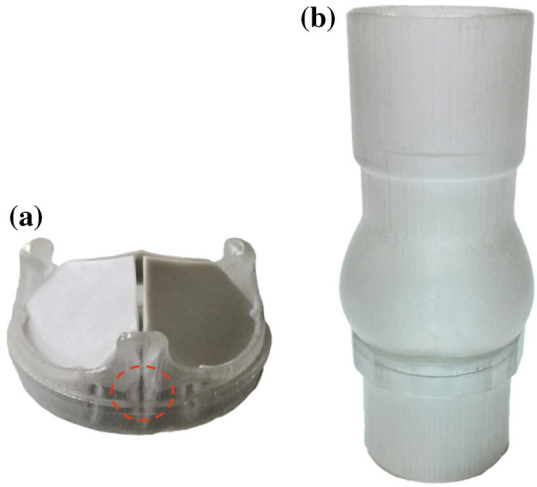


**FIGURE 4. Transparent 3D-prints of the valve housing with assembled leaflets (a) and the model of the aortic root (b). The pivoting region is indicated by a red circle.**

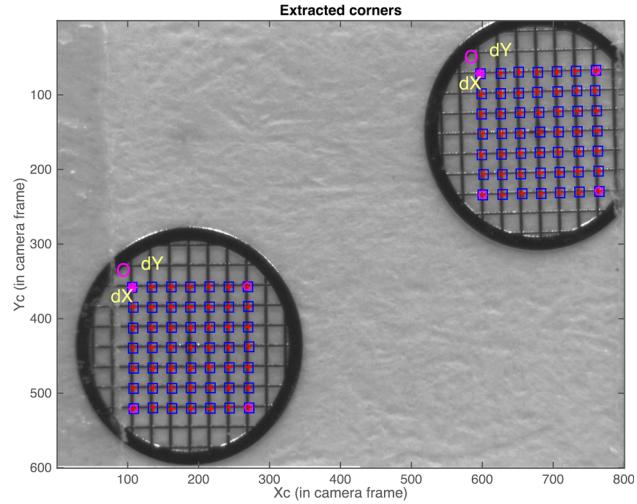


**FIGURE 5. Calibration targets at two positions in the frame. The optical distortions remained below 1 pix throughout the image.**

mm$^2$) and has a refractive index of 1.48 at the wavelength of the illumination. This technique has several advantages over traditional silicone casting as it allows to resolve even very small structures and complex geometries of the model while maintaining its functional integrity (Fig. 4).

### *Illumination and Optics*

The scene was captured by a high-speed camera (Phantom v12.1, Vision Research Inc., Wayne, NJ, USA) with a Nikkor 100 mm f2.8 macro lens together with some extension tubes to reach the final magnification of 2.46. The depth of field (DOF) of the optical setup was 0.5 mm which is so narrow that only a thin layer of particles will be in focus, but large enough to cover the whole depth of the measurement location. So, rather than using a light sheet, as in traditional PIV, volume illumination of the scene is used and layer isolation is done purely by the optics. Optical distortions of the camera and lens system were assessed in air outside of the test section using precision calibration targets with a pitch of 250 $\mu$m normally used for electron microscopy (TG100Ni, EM Resolutions Ltd., Essex, UK). The calibration target was not large enough to cover the whole field of view which is why multiple target locations were superimposed to obtain the distortion coefficients in the full field of view. The distortions of the images were very low and remained below 1 pix in the image corners (where the lens distortions are most noticeable). Figure 5 shows two calibration targets at critical corner locations. Outside calibration in air is common practice in $\mu$PIV applications due to limited access to the interior of the test section. It requires a good index matching between the test fluid and the material of the test section. The camera recorded at 10,000 FPS with 800 $\times$ 600 pixels, in a resolution of 8.2 $\mu$m/pix. Pulsed illumination at a frequency of 10 kHz is not possible with most currently available lasers. Therefore, we made use of a recently developed technique in which high-power LED pulses are used for localized volume illumination. It was found that LED modules can be driven with current pulses that are well above the LED's continuous current rating as long as the pulses are short and the duty cycle remains low.[23] In the present case, the LED module was driven with 3 $\mu$s pulses of 150 $A$. The light from the LED module (CBT-120, Luminus Devices Inc., Woburn, MA, USA) was transmitted to the area of interest *via* fiber optics for spot illumination. This enabled us to sufficiently illuminate the scene and obtain velocity fields at a high rate to resolve the fast dynamics of the flow and the valve. The use of fluorescently labeled tracer particles together with a matching filter pair allowed to remove most of the background light from the flow images so that the camera only captured the fluorescence signal from the tracer particles. A second high-speed camera (Fastcam Mini UX100, Photron USA Inc., San Diego, CA, USA) was mounted at a higher position than the PIV camera with a downward angle such that all three leaflets are visible in the frame (in contrast to camera 1 with only two leaflets in the field of view) to study the dynamics of all three individual leaflets.

### *Test Fluid*

A mixture of glycerol, water, and sodium iodide (19/23.5/57) wt% served as a blood analog matching both

the kinematic viscosity of blood of 3.5 cSt as well as the refractive index (RI) of the transparent housing of 1.48. Matching the RIs of the different materials eliminates optical distortions at the interfaces of the different media and ensures reliable particle identification for PIV. A convex lens shape was printed from the transparent housing material to perform index matching. Immersed in plain water, this lens yielded strong distortions (Fig. 6a), while the same lens immersed in RI-matched blood analog showed almost no sign of optical distortion (Fig. 6b). A small amount of sodium thiosulfate (0.5 wt%) was added to prevent decomposition of the sodium iodide in the fluid.

Micro particle image velocimetry imposes special requirements on the particle seeding as the field of view is very small compared to the total volume of fluid. To have a sufficient number of tracer particles in each frame, either the seeding density has to be increased well beyond typical levels used in macroscopic PIV, or images from multiple phase-locked realizations of the experiment have to be combined. The latter is difficult to achieve because there are moving components in the frame (valve leaflets) and the required temporal resolution is high. Variations in leaflet motion of just a few milliseconds can make processing difficult and the results become prone to errors. Increasing the seeding density results in a significant increase in cost as small fluorescent tracer particles for $\mu$PIV are expensive. In our study, we were able to make use of self-made Rhodamine-B tracer particles which could be manufactured at a much lower cost and were available at sufficient quantity. The high particle count enabled capturing flow images with sufficient tracer density in one run without the need for phase averaging. The particles were manufactured according to Pedocchi *et al.*[14] and had an average size of 35 $\mu$m and a density of 1.2 g/cm$^3$. The peak in the excitation spectrum for these particles is at 554 nm and the peak in the emission spectrum is at 579 nm in water. The shift between excitation and emission spectrum (Stokes shift) allows to separate the emission signal from the excitation signal with a matching filter pair.

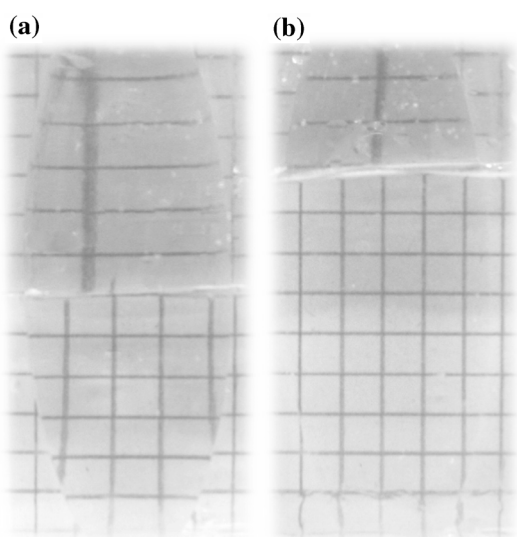


**FIGURE 6. A VeroClear printed lens (with a grid in the background for optical reference) immersed in water (a) and in RI-matched fluid (b) allowed to assess the optical distortions and to perform index-matching. Strong distortions at the edges of the printed lens (a). In case (b) the only noticeable distortions at the bottom are due to residue from the silicone sealing on the container wall.**

### *Processing*

High-speed flow imaging produces large data streams (10 GB/s in the present case) to be stored and processed. This requires a high degree of automation, together with powerful computers to process the data in reasonable time. Our workflow was optimized towards minimal user interaction and efficient data handling for "over-night" processing. Moving background images were created dynamically and then subtracted from the flow images. Each PIV interrogation window was populated on average by 5 tracer particles which is below the optimal seeding density. A correlation average was computed on subsequent frames to improve the quality of the correlation maps and to obtain a densely populated vector field. The correlation average was not calculated over multiple realizations of the experiment, but over subsequent frames of the same sequence. This amounts to a low-pass filtering of the flow signal by moving window

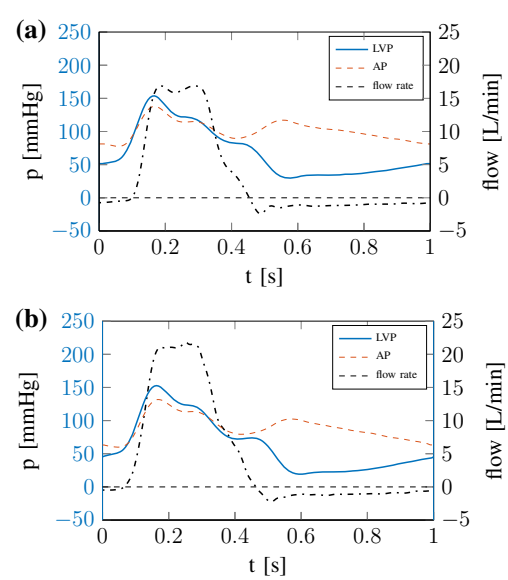


**FIGURE 7. Flow and pressure profiles for CO = 3.0 L/min (a) and CO = 4.5 L/min (b).**

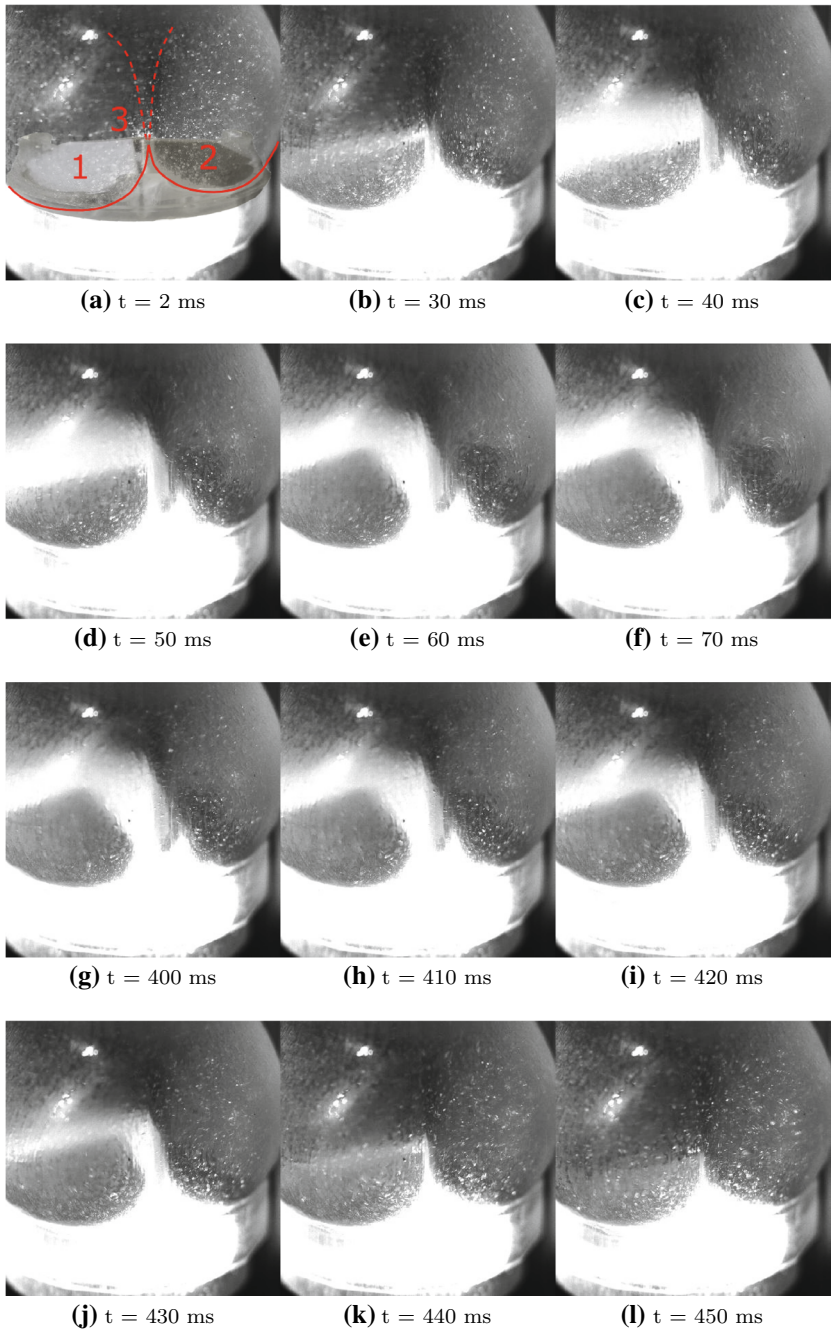


**FIGURE 8. Leaflet position (1–3, as indicated in the first frame) at various time instances. Leaflet motion is very synchronous during the closing phase with an average closing time of 55 ms. The main flow direction is bottom to top. Full movie provided in the supplementary material.**

averaging. The employed method is described in detail in Sciacchitano *et al.*[17] Given a sample rate of 10 kHz and a correlation average over 26 frames, we were still able to resolve all of the transient effects at the time scales of the cardiac flow. PIV was performed based on a grid-refinement algorithm in which the final window size was 32 × 48 pixels with 50/66 % overlap. In metric units this amounts to a spatial resolution of 0.13 mm. Together with a temporal resolution of 0.1 ms this allowed the study of the fast valve dynamics.

### *Uncertainty Analysis*

The viscous shear stress (VSS) is an important parameter when analyzing a heart valve's thrombogenic potential and is given as:

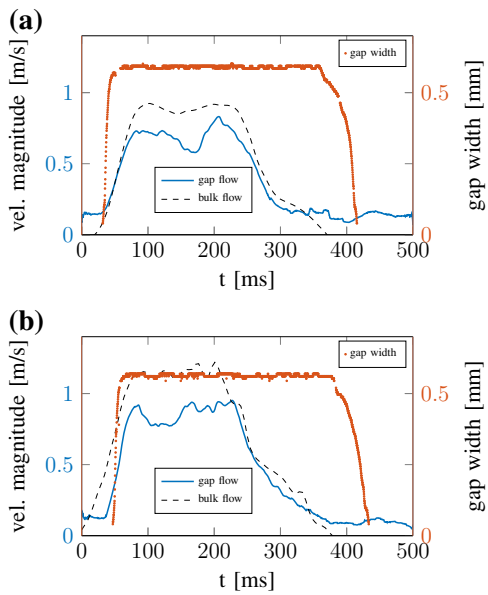


**FIGURE 9. Gap flow, gap width and bulk flow for CO = 3.0 L/min (a) and CO = 4.5 L/min (b).**

$$VSS = \mu\left(\frac{\partial U}{\partial y} + \frac{\partial V}{\partial x}\right) \quad (1)$$

where $\mu$ is the dynamic viscosity and $U$ and $V$ are the velocity components in the horizontal and vertical direction respectively. The uncertainty in velocity was calculated from the minimal detectable particle shift, divided by the time step between exposures. It was computed as $\Delta U = \Delta V = 0.0244$ m/s assuming 0.3 pix minimum detectable shift (subpixel interpolation). A histogram analysis of the PIV data showed that the velocity computation is unlikely to be affected by peak-locking. The uncertainty in dynamic viscosity $\mu$ due to errors in mixture and temperature variations during the experiments was estimated to be $\Delta\mu = 0.035$ cP. This results in an uncertainty for the VSS calculation of $\Delta VSS = 6.57$ Pa.

## RESULTS

Two flow configurations with cardiac outputs (CO) of 3.0 L/min and 4.5 L/min respectively at a heart rate of 60 BPM and a systolic to diastolic pressure ratio of 140/80 mmHg were evaluated. The corresponding flow and pressure profiles are depicted in Fig. 7. The fluid temperature was kept at 30 °C for which the required viscosity of $\nu = 3.5$ cSt and the required RI of 1.48 are obtained. This temperature is higher than the ambient temperature to allow for thermal dissipation of heat that may be introduced into the system by the pump.

### *Valve Dynamics*

Figure 8 shows snapshots at various time points during valve opening (a–f) and valve closure (g–l) for the high cardiac output case (CO = 4.5 L/min). These images were recorded with the second high-speed camera showing all three leaflets (see also the supplementary material for a movie of the opening and closing valve). Panels (a) through (f) show asynchronous opening of the leaflets where leaflet 1 (cf. Fig. 8) opens later than leaflets 2 and 3. Individual leaflets opened as fast as 18 ms and the opening of all three leaflets was completed within 40 ms on average. No fluttering of the leaflets could be detected during the fully-open phase. The closing behavior was very different from the opening: the three individual leaflets closed in a synchronous manner with only small variance which is in good agreement with Brücker *et al.*[2] The closing was much slower than the opening with an average closing time of 55 ms, independent of the CO. The valve leaflets have a closing angle of 35° and opened to a maximum opening angle of 85° which is in accordance with Brücker *et al.*[2]

### *Flow Dynamics*

A small gap between the leaflet ear and the flange of the housing exists during systole (Fig. 2). Figure 9 shows bulk flow, gap flow and gap width, plotted over time, where the gap flow was measured with $\mu$PIV and the bulk flow velocity was calculated from the flow sensor reading. The instantaneous gap width was determined from the flow images. The gap width is a function of the leaflet kinematics and one can see from Fig. 9 the slow (55 ms) leaflet closure for both CO at $t \approx 400$ ms. The gap flow showed to closely follow the bulk flow throughout the cardiac cycle and one can distinguish between various flow phases. The first phase is dominated by the acceleration of the fluid and the opening of the valve. The flow accelerates at a higher rate in the high CO case which also reflects on the gap flow. This is followed by a phase of nearly constant maximum velocity through the gap in the fully-open leaflet position. The maximum velocity in the gap was extracted from the PIV data and was found to be on the order of 1 m/s for 4.5 L/min CO and 0.8 m/s for 3.0 L/min CO respectively. During mid-systole strong vortices in the sinus portions are forming (see movie in the supplementary material) which are believed to support the smooth closure of the valve.[1] With decelerating bulk flow the gap flow also starts decelerating at $t \approx 250$ ms until the flow direction of bulk flow and gap flow are reversed at $t \approx 400$ ms. The valve closes tightly in the pivot and no flow could be observed in the pivoting region during

diastole. The FURTIVA valve features a "Mercedes star" design which his is a star-shaped cut-out at the central leaflet edges resulting in a small leakage. This feature of the valve is designed to prevent a high-velocity jet of reverse flow through a small central gap during the late closure of the valve by geometrically imposing a minimum gap width between the leaflets. This central leakage during diastole is likely the most critical site for potential elevated shear stresses during diastole.

### *Viscous Shear Stress*

The pivoting region (Fig. 1d) is a region of potentially high shear stresses and thus requires quantitative assessment. Following the approach by Jun *et al.*[7] we calculated the viscous shear stress (VSS) within the flow field which is known to be linked to thrombogenicity. Figure 10 shows the velocity map and the VSS in the pivoting region at characteristic times during the systolic phase. The flow velocity continuously increases during valve opening (a–i) until it reaches its maximum value of approximately 1 m/s. With increasing velocity, the VSS increases and regions of locally elevated shear evolve. These hot spots show a maximum VSS of approximately 20 Pa during maximum forward flow (k–l). A closer look at the VSS map in panel (l) indicates that these hot spots are in the regions close to the flange and the leaflet ear. These two geometric features function as an obstruction to the high velocity fluid which is deflected towards the pivot causing an increase in viscous shearing. This situation remains throughout the quasi-stationary constant flow phase of mid-systole (t $\approx$ 75–250 ms). From t $\approx$ 250 ms onwards the flow decelerates resulting in a reduction of VSS. The valve starts closing with beginning reverse flow at t $\approx$ 400 ms. The reverse flow reaches velocities on the order of 0.2 m/s which is five times slower than the peak forward flow (o–x). This low velocity results in significantly reduced VSS in the pivoting region during valve closure staying below 10 Pa throughout the picture (notice the change of scales in velocity maps and VSS maps).

The leaflet ear has been identified as a region of elevated shear stresses in the time-resolved PIV analysis. Here, the quasi-stationary phase of mid-systole showed the highest VSS when velocity gradients and flow deflection are maximal. These PIV results offer a high temporal resolution, but the spatial resolution in the narrow regions was limited. A spatially more detailed view of the previously identified critical sites during mid-systole was obtained from particle tracking velocimetry (PTV). By averaging the flow in time during the quasi-stationary flow phase (as seen from the temporal PIV data), we obtained a velocity map with much higher resolution that gives a more detailed view of the velocity field in the critical, narrow regions. This hybrid PIV/PTV approach allows to resolve the transient effects with high temporal resolution while providing a high spatial resolution during the quasi-stationary phase. Figure 11a depicts a velocity map obtained from PIV with the region of interest (ROI) for PTV indicated. The PTV data interpolated onto a regular grid with a spacing of 50 $\mu$m confirms that the gap flow is deflected by the leaflet ears in its entrance region and follows the contours of the leaflet and the flange (Fig. 11b). The spatially finely resolved flow field showed the highest velocities in form of a jet-like flow along the leaflet ear in the central region of the gap and reached velocities of up to 1.06 m/s for CO = 4.5 L/min. This jet is slightly shifted from the gap center line towards the leaflet side. The VSS in this narrow region is shown in Fig. 11c and confirms the location of the highest VSS at the tip of the leaflet ear with VSS values up to 40 Pa.

**FIGURE 10. Evolution of flow field and viscous shear stress during the systolic phase. Colors of velocity maps inverted for better readability.** ▶

## DISCUSSION

The combination of several novel experimental technologies (e.g. high-power LED illumination, 3D-printed aortic root model) made it possible to perform transient flow measurements on small scale and at high frequency which allowed to resolve and study the fast valve dynamics during the cardiac cycle which often remains inaccessible to traditional techniques. The Lapeyre-Triflo FURTIVA mechanical heart valve showed synchronous and slow closing of the valve leaflets with no apparent systolic regions of flow stagnation in the pivoting region. The measured valve closing is considerably slower than in classical mechanical heart valves and is consistent with Li *et al.*[10] and Lu *et al.*[13] High closing velocities of MHVs can lead to formation of cavitation bubbles and severe blood damage. The slow closure of the Triflo valve as seen here is expected to be hemodynamically beneficial[10,12] and cavitation is unlikely. The measured flow velocities in the pivoting region did not exceed 0.8 m/s or 1.0 m/s for the two studied cases. Simon *et al.*[19] published experimental data on the hinge flow for a 23 mm St. Jude Mechanical (SJM) and a CarboMedics (CM) valve obtained from laser doppler velocimetry (LDV). In the aortic position the SJM showed a maximum velocity in the hinge of 1.75 m/s and the CM valve showed up to 2.31 m/s during peak systole. In a later work Simon *et al.*[18] performed a three-dimensional simulation of the hinge flow field of a St. Jude Medical bileaflet mechanical heart valve. They found

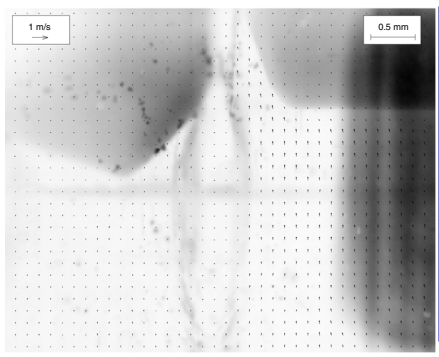


**(a)** t = 30 ms

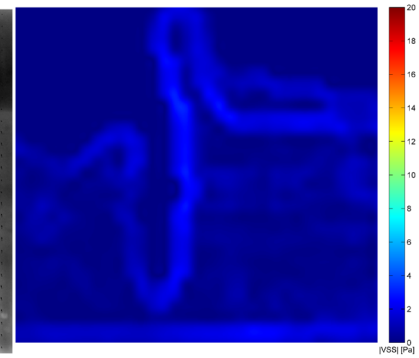


**(b)** t = 30 ms

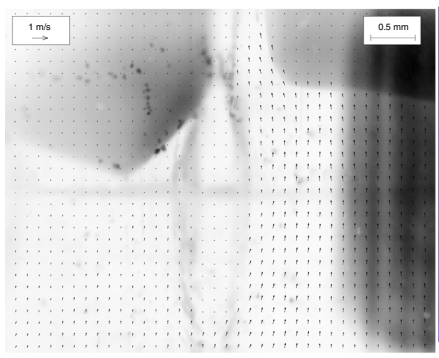


**(c)** t = 40 ms

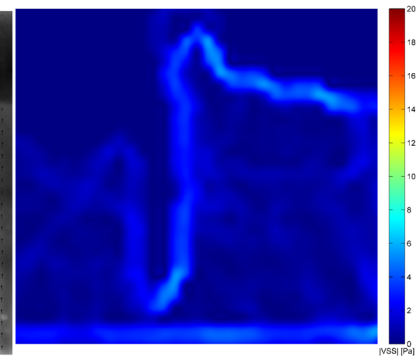


**(d)** t = 40 ms

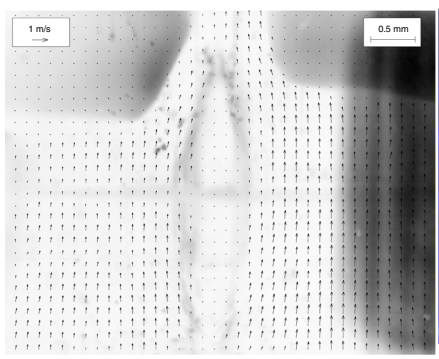


**(e)** t = 50 ms

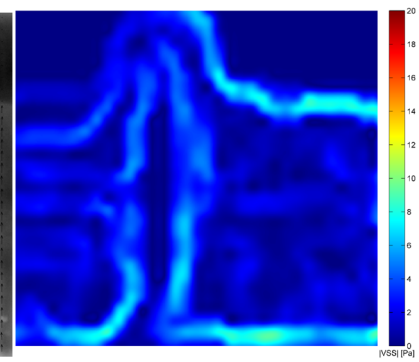


**(f)** t = 50 ms

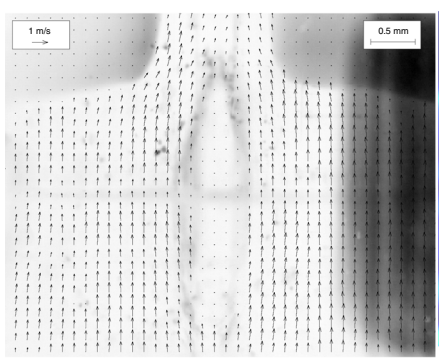


**(g)** t = 60 ms

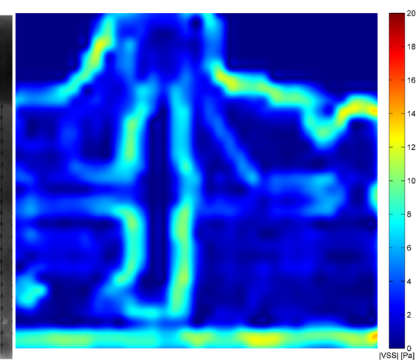


**(h)** t = 60 ms

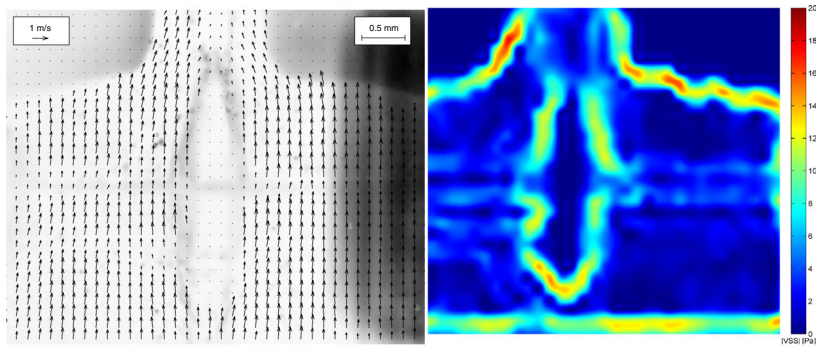


**(i)** t = 70 ms **(j)** t = 70 ms

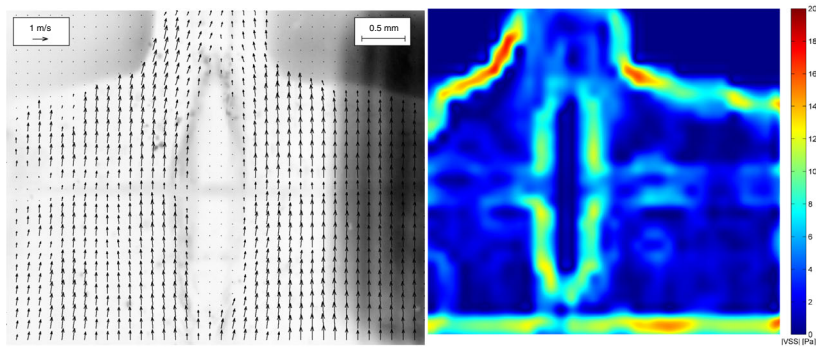


**(k)** t = 100 ms **(l)** t = 100 ms

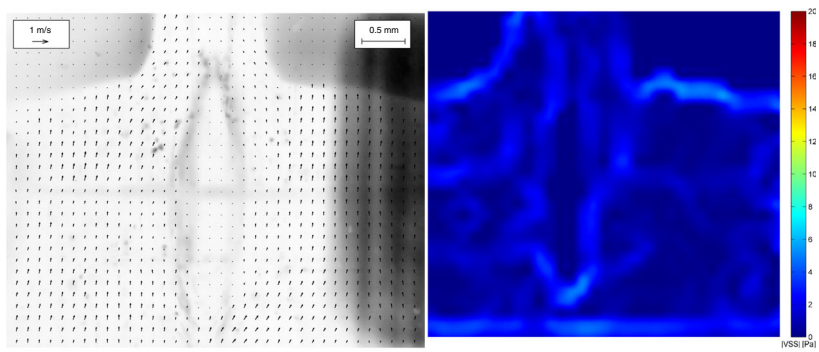


**(m)** t = 300 ms **(n)** t = 300 ms

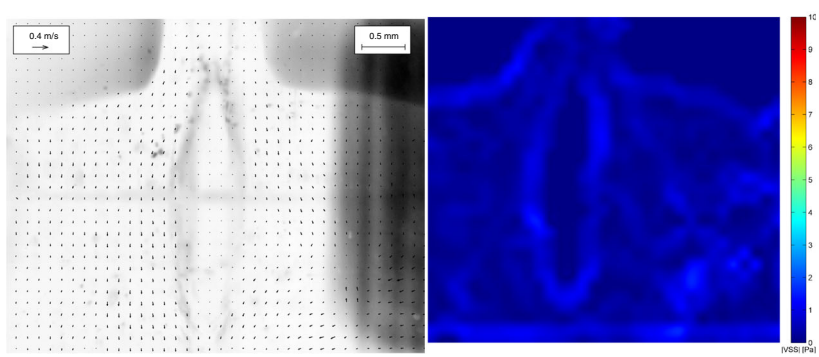


**(o)** t = 400 ms **(p)** t = 400 ms

**FIGURE 10. continued**

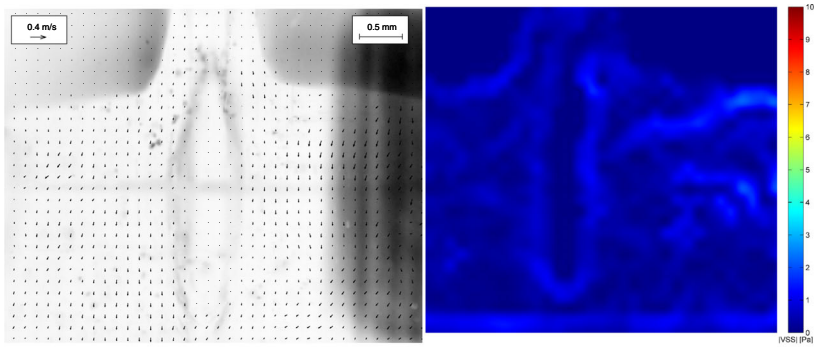


**(q)** t = 410 ms **(r)** t = 410 ms

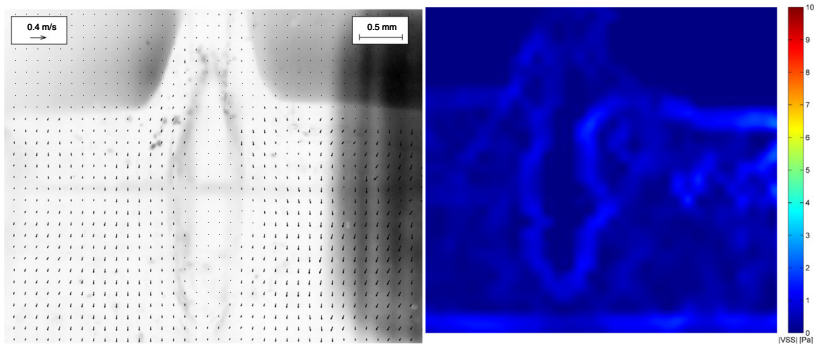


**(s)** t = 420 ms **(t)** t = 420 ms

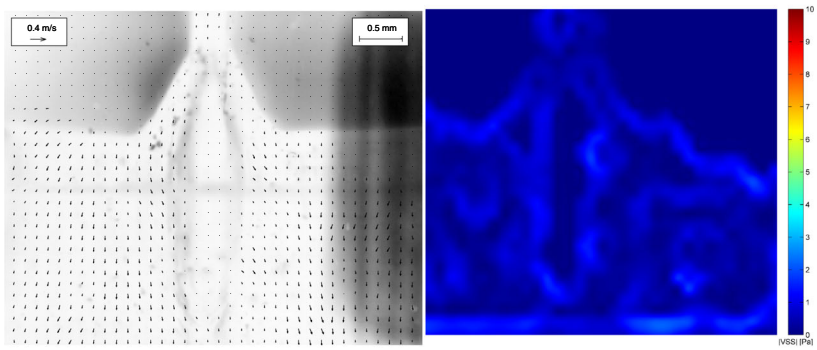


**(u)** t = 430 ms **(v)** t = 430 ms

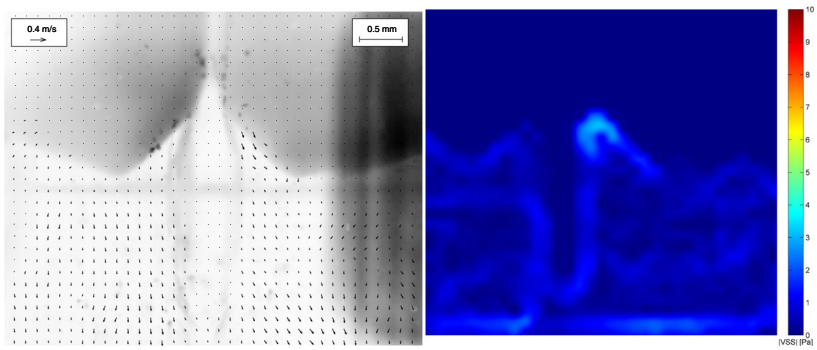


**(w)** t = 440 ms **(x)** t = 440 ms

**FIGURE 10. continued**

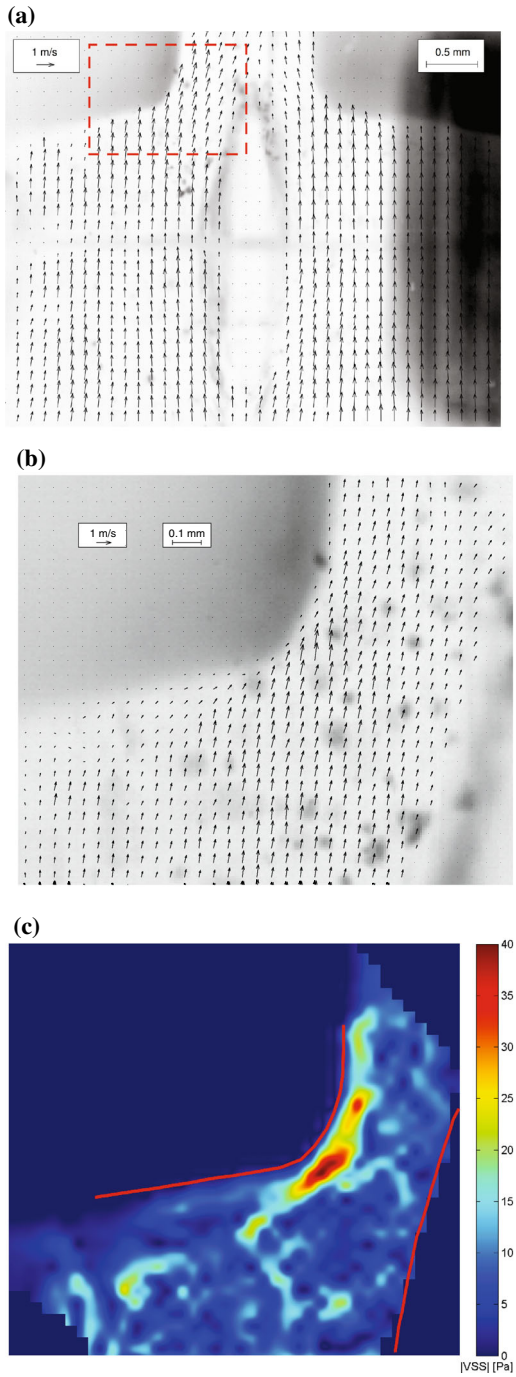


**FIGURE 11. Inverted greyscale PIV image during systole with region of interest for PTV indicated (a). The velocity fields from PIV (a) and PTV (b) are determined from the relative particle shift between two subsequent frames. A hot spot with elevated VSS on the order of 40 Pa was identified at the tip of the leaflet ear (c).**

that the hinge flow closely follows the valvular flow which was also found in our study and saw maximum systolic hinge flow during peak systole with velocities up to 1.54 m/s. All of the measured velocities are at least 50 % higher than what we measured for the Triflo valve. Furthermore, Simon *et al.*[18] reported a pocket of reverse flow at the bottom of the hinge during forward flow. This was not observed for the Triflo valve and it can be hypothesized that this may be an indicator for reduced thrombogenic risk of the Triflo valve during systole. The data that can be found in the literature on fluid velocities in the hinge region of aortic MHVs during the systolic phase is limited because for classical MHV designs the diastolic phase is more critical regarding high velocity jets and elevated shear. Jun *et al.*[7] reported velocities of up to 3.6 m/s during the diastolic phase of a St. Jude Medical regent valve. Klusak *et al.*[9] measured velocities up to 5.7 m/s in a model of a bileaflet mechanical heart valve during reverse flow. The Lapeyre-Triflo FURTIVA valve was found to behave fundamentally different due to its novel hinge design. No flow through the pivoting region could be observed during diastole. From these findings it can be concluded that unlike MHVs that feature a classical hinge design, the FURTIVA valve shows maximal VSS in its pivoting region during mid-systole forming hot spots at the flanges and the leaflet ears with VSS up to 40 Pa for the given flow conditions. This is below the commonly used threshold for platelet activation. The high spatial resolution of the PTV analysis yields a good estimate of the VSS because the velocity gradients are well resolved. The temporal PIV analysis is limited in its ability to resolve the fine-scale gradients resulting in an underestimation of the VSS. However, the temporal $\mu$PIV technique proved to be a valuable tool for the localization of hot spots of elevated shear, which were then studied in more detail with PTV, and for the analysis of their temporal evolution. As in every tightly closing valve, there are also zones of local flow stagnation during diastole. However, we did not observe regions of flow stagnation that are in close spatial and temporal vicinity to regions of elevated shear and washout of the pivoting area was provided during each cycle.

It was beyond the scope of this study to investigate the leakage situation and the VSS in regions that lie outside the pivoting region as previously defined. The peripheral gaps between the edges of the leaflets and the valve housing should receive further attention and should be analyzed for their thrombogenic behavior. We expect the major portion of the leakage flow to pass through the central star-shaped gap (see "Mercedes star" gap in Fig. 1d) of the valve during diastole and this gap should be considered when assessing the diastolic thrombogenic potential of the Triflo valve. A rough estimation of the expected VSS in the central gap of the valve showed that the threshold for platelet activation may be exceeded during beginning diastole.

In summary, no critical combinations of regions of flow stagnation and zones of excessive shear were observed in the pivoting region and we conclude that the investigated pivoting region of the Triflo valve showed favorable hemodynamics with low potential for thrombogenic events.

## ELECTRONIC SUPPLEMENTARY MATERIAL

The online version of this article (doi: 10.1007/s13239-016-0264-z) contains supplementary material, which is available to authorized users.

## ACKNOWLEDGMENTS

The authors would like to thank Triflo Medical Switzerland Sarl for providing us with the Lapeyre-Triflo FURTIVA valve used in this project.

## CONFLICT OF INTEREST

Bernhard M. Vennemann, Thomas Rösgen, Thierry P. Carrel and Dominik Obrist declare that they have no conflict of interest.

## ETHICAL APPROVAL

No human and animal studies were carried out by the authors for this article.

## REFERENCES

[1]Bellhouse B. J. and F. H. Bellhouse. Mechanism of closure of the aortic valve. Nature 217: 86-87, 1968.

[2]Brucker C., U. Steinseifer, W. Schroder and H. Reul. Unsteady flow through a new mechanical heart valve prosthesis analysed by digital particle image velocimetry. Meas. Sci. Technol. 13: 1043-1049, 2002.

[3]Gallegos R. P., A. L. Rivard, P. T. Suwan, S. Black, S. Bertog, U. Steinseifer, A. Armien, M. Lahti and R. W. Bianco. In-vivo experience with the Triflo trileaflet mechanical heart valve. J. Heart Valve Dis. 15: 791-799, 2006.

[4]Govindarajan V., H. S. Udaykumar and K. B. Chandran. Two-dimensional simulation of flow and platelet dynamics in the Hinge region of a mechanical heart valve. *J. Biomech. Eng. T ASME* 131, 2009.

[5]Gregoric I. D., K. Eya, D. Tamez, R. Cervera, D. Byler, J. Conger, E. Tuzun, H. K. Chee, F. J. Clubb, K. Kadipasaoglu and O. H. Frazier. Preclinical hemodynamic assessment of a new trileaflet mechanical valve in the aortic position in a bovine model. J. Heart Valve Dis. 13: 254-259, 2004.

[6]Hoffmann G., G. Lutter and J. Cremer. Durability of bioprosthetic cardiac valves. Dtsch. Arztebl. Int. 105: 143-148, 2008.

[7]Jun B. H., N. Saikrishnan and A. P. Yoganathan. Micro particle image velocimetry measurements of steady diastolic leakage flow in the hinge of a St. Jude Medical(R) regent mechanical heart valve. Ann. Biomed. Eng. 42: 526-540, 2014.

[8]Kaufmann T. A., T. Linde, E. Cuenca-Navalon, C. Schmitz, M. Hormes, T. Schmitz-Rode and U. Steinseifer. Transient, three-dimensional flow field simulation through a mechanical, trileaflet heart valve prosthesis. ASAIO J. 57: 278-282, 2011.

[9]Klusak E., A. Bellofiore, S. Loughnane and N. J. Quinlan. High-resolution measurements of velocity and shear stress in leakage jets from bileaflet mechanical heart valve Hinge models. J BIOMECH ENG-T ASME 137,2015.

[10]Li C. P., S. F. Chen, C. W. Lo and P. C. Lu. Turbulence characteristics downstream of a new trileaflet mechanical heart valve. ASAIO J. 57: 188-196, 2011.

[11]Li C. P. and P. C. Lu. Numerical comparison of the closing dynamics of a new trileaflet and a bileaflet mechanical aortic heart valve. J. Artif. Organs 15: 364-374, 2012.

[12]Lu C. P. et al., The closing behavior of mechanical aortic heart valve prostheses. ASAIO J. 50:294-300, 2004.

[13]Lu C. P. and P. C. Li, Numerical comparison of the closing dynamics of a new trileaflet and a bileaflet mechanical aortic heart valve. J. Artif. Organs 15:364-374, 2012.

[14]Pedocchi F., J. E. Martin and M. H. Garcia. Inexpensive fluorescent particles for large-scale experiments using particle image velocimetry. Exp. Fluids 45: 183-186, 2008.

[15]Roudaut R., K. Serri and S. Lafitte. Thrombosis of prosthetic heart valves: diagnosis and therapeutic considerations. Heart 93: 137-142, 2007.

[16]Sato M., H. Harasaki, K. E. Wika, M. V. Soloviev and A. S. Lee. Blood compatibility of a newly developed trileaflet mechanical heart valve. ASAIO J. 49: 117-122, 2003.

[17]Sciacchitano A., F. Scarano and B. Wieneke. Multi-frame pyramid correlation for time-resolved PIV. Exp. Fluids 53: 1087-1105, 2012.

[18]Simon H. A., L. Ge, I. Borazjani, F. Sotiropoulos and A. P. Yoganathan. Simulation of the three-dimensional hinge flow fields of a bileaflet mechanical heart valve under aortic conditions. Ann. Biomed. Eng. 38: 841-853, 2010.

[19]Simon H. A., H. L. Leo, J. Carberry and A. P. Yoganathan. Comparison of the hinge flow fields of two bileaflet mechanical heart valves under aortic and mitral conditions. Ann. Biomed. Eng. 32: 1607-1617, 2004.

[20]Steinseifer U., C. Schmitz, T. Linde, T. Kaufmann and T. Schmitz-Rode. The Triflo trileaflet mechanical heart valve: design and in vitro performance. Int. J. Artif. Organs 32: 400-400, 2009.

[21]Swanson W. M. and R. E. Clark. Dimensions and geometric relationships of human aortic value as a function of pressure. Circ. Res. 35: 871-882, 1974.

[22]Turina M., Supra-annular aortic valve replacement with a mechanical prosthesis Multimed. Man. Cardiothorac Surg. 1129:000083, 2005.

[23]Willert C., B. Stasicki, J. Klinner and S. Moessner. Pulsed operation of high-power light emitting diodes for imaging flow velocimetry. Meas. Sci. Technol. 21:075402, 2010.